CONCLUSIONS

Based on the data presented herein, for a selected set of parameters, it is determined that the isotherm and streamline contours are rather insensitive to the actual shape of the energy generation rate function although their magnitudes are affected. The linear-positive-slope profile produced the coolest annulus and consequently the one circulating the most slowly. This is characteristic of profiles which peak near the outer sphere. The local wall heat flux results show that the northern regions of the outer sphere are subject to the major thermal stress. On the inner sphere, the northern latitudes are also the hottest.

REFERENCES

1. J. Nelsen, R. Douglass and D. Alexander, Natural convection in a spherical annulus filled with heat generating fluid, *Proc. 7th Int. Heat Transfer Conf.*, Vol. 2, pp. 171–176 (1982).
2. J. Nelsen, Natural convection of heat generating fluid in spherical annuli, M.S. thesis, University of Nebraska, Lincoln, Nebraska (1981).
3. J. M. Nelsen and R. W. Douglass, On partial spectral expansions using natural convection in spherical annulus enclosures as an example, *Numerical Heat Transfer* **6**, 67–84 (1983).

Int. J. Heat Mass Transfer. Vol. 27, No. 10, pp. 1928–1932, 1984
Printed in Great Britain

0017-9310/84 $3.00 + 0.00

Transport from a vertical ice surface melting in saline water

R. S. JOHNSON
Harrison Radiator Division, General Motors Corporation, Lockport, NY 14094, U.S.A.

and

J. C. MOLLENDORF
Mechanical and Aerospace Engineering, State University of New York at Buffalo, Amherst, NY 14260, U.S.A.

(*Received* 9 *February* 1983 *and in revised form* 20 *January* 1984)

INTRODUCTION

THE IMPORTANCE of ice–seawater interactions has been evident since the early investigation of Sandström [1]. Later, Neshyba [2] suggested that the upwelling produced by melting icebergs could strongly influence the supply of nutrients to Antarctic surface waters.

In saline water, the coupled effects of thermal and saline diffusion, on the motion-causing buoyancy force, results in considerable added complexity. Previous work dealing with the melting of ice in pure water has been summarized by Carey and Gebhart [3, 4], and includes abstracts of papers presented at meetings by Josberger and Martin [5] and Josberger [6] who have considered the buoyancy-induced flow near ice in seawater. In a more complete discussion of their work, Josberger [7, 8] and Josberger and Martin [9] report observations regarding vertical ice slabs melting in sea water. It was observed that next to the ice surface, upwardly flowing fluid began as laminar then developed into turbulence, where the transition location was governed by a saline Grashof number. Also, in the laminar regime, they observed bidirectional flow, with an upward inner flow and downward outer flow. They presented measured interface temperatures found by freezing themistors in the ice, but the effect of internal heat conduction in the ice is not clear. Strikingly increased local melting rates were observed in the transition region where the flow went from a bidirectional laminar flow to an upward turbulent flow. In this region, a 'notch' was formed in the ice as the entrained fluid divided to feed the upward and downward flows. Such a 'notch' was also seen in the work reported by Sandstrom [1].

Marschall [10] solved the boundary-layer equations governing heat, mass and momentum transfer and presented results for the relationships between interface temperature, ambient temperatures and interface salinity.

Carey and Gebhart [3, 4] numerically computed boundary-layer flow and transport adjacent to a vertical ice surface in saline water for a wide range of ambient salinities and temperatures. Their calculations show excellent agreement with the results of Josberger [8] and those from the present paper. They also conducted vertical ice melting experiments in $10^{\circ}/_{\circ\circ}$ saline water over the ambient temperature range of 1–15°C and showed, by a time exposure photographic technique, the nature of the natural convection flows.

EXPERIMENTAL APPARATUS AND PROCEDURE

Nominally, the present experiment consisted of melting a vertical, bubble-free ice slab of dimensions 30.3 cm high by 14.8 cm wide with an initial thickness of 3 cm in saline water at a concentration of about $35^{\circ}/_{\circ\circ}$. The actual ambient salinity ranged between 34.5 and $35.5^{\circ}/_{\circ\circ}$.

Frozen in the ice slab were five thermocouples to both measure the ice–liquid interface temperature, t_{il}, during melting; and, before a run, to determine when the entire slab was at the t_{il} temperature expected to result for the given ambient temperature. Equilibrium was obtained by 'over-freezing' the ice to a temperature below the expected t_{il} temperature for each individual experimental run. The ice was then put into an insulated box and allowed to warm slowly to the expected t_{il}. This procedure insured negligible internal conduction and consequently a very accurate inference of the interfacial melting temperature. This is necessary, since it would be difficult to separate out transient internal conduction effects accurately.

The artificial seawater was made according to a precise recipe given by Lyman and Fleming [11]. The salinity was checked continually by comparing the electrical conductivity of the tank water with that of a sample of seawater made from the recipe. In addition, the recipe solution was found to be within $0.2^{\circ}/_{\circ\circ}$ of a standard sample of seawater, obtained from the Institute of Oceanographic Sciences in Wormley, Godalming, Surrey, U.K. Using the measured electrical conductivity of the seawater, the salinity was calculated using the Joint Panel on Oceanographic Tables and Standards, see Cox [12].

Before each run, the ambient water was made thermally uniform by stirring vigorously for a few hours, then allowing the water to reach a quiescent state. Thermocouples were used to monitor the degree of thermal stratification. The maximum acceptable level of stratification was typically less than $0.2^{\circ}C\ m^{-1}$. This corresponds closely to the maximum density gradient in the Weddell Sea, 1.65×10^{-7} g cm^{-3} cm^{-1}, reported by Neshyba [13]. The ambient temperature level was measured using a precision mercury-in-glass-thermometer with 0.1° divisions, located at midheight in the tank about 10 cm from the tank wall.

In addition to inferring flow direction using differential thermocouples, the flow was also observed using a Schlieren optical system. Photographs were taken with 400 ASA Tri-X film using a Nikkormat 1 : 1.4 camera. Back lighting of the ice slab arrangement was used to determine the location of the frame with respect to the ice extending from it.

RESULTS

After immersion, the instantaneous weight of the suspended slab was recorded. The weight change was found to be linear with time. The melting rate is related to the weight change as follows:

$$\dot{m} = \left[\frac{\rho_{ice}}{\rho_{\infty}(t_{\infty}, s_{\infty}, p_{\infty}) - \rho_{ice}}\right]\dot{M}. \quad (1)$$

Equation (1) differs from that used by Bendell and Gebhart [14] in that they incorrectly used ρ_{∞} instead of ρ_{ice} in the numerator of equation (1). This amounts to about a 9% overestimate of the measured melting rate, heat transfer and Nusselt number $\overline{Nu}$. Their results therefore, should be corrected by multiplying them by ρ_{ice}/ρ_{∞}.

It was found that, for the present saline water data, the heat transfer decays monotonically with decreasing t_{∞} for the range of t_{∞} considered, see Johnson [15]. This is in contrast with the present pure water results, the corrected results of Bendell and Gebhart [14] and the laminar theory of Gebhart and Mollendorf [16]. In each of these investigations, a minimum in $\overline{Nu}$ was found for pure water. The present pure water data is also seen to agree well with the revised data of Bendell and Gebhart [14]. As will be seen later, for ice melting in $35^{\circ}/_{\circ\circ}$ saline water, the flow undergoes unusually early (in terms of a purely thermal Grashof number) transition from laminar to turbulent flow with the laminer portion length decreasing with increasing t_{∞}. Because of this, the average Nusselt number determinations given in Johnson [15] represent combined laminar and turbulent transport, to varying degrees, depending upon t_{∞}.

The direction in which the fluid flows is controlled by many mechanisms, and, if there is a tendency for bidirectional flow, transition-to-turbulence may be greatly influenced. The dominant buoyancy mechanisms are the effect of the temperature and salinity differences on density. In an assessment of a buoyancy-induced flow, the appropriate definition of the Grashof number, Gr, is of considerable importance. For example, in analysis it suggests physical limits of applicability inasmuch as its magnitude determines when certain terms in the governing equations may be neglected. In connection with this, the Grashof number also bears directly on the characteristic, or scaling velocity, $U_c = (\nu/x)\sqrt{Gr}$. It is not a simple matter, however, to select the proper representative Grashof number for the kinds of flows considered here. There are multiple and opposed buoyancy forces. In general, the Grashof number may be defined as the 'unit Grashof number', gx^3/ν^2, times a measure of the units of buoyancy, $\Delta\rho/\rho_r$, where ρ_r is the density evaluated at some appropriate reference condition. Several possible Grashof numbers include

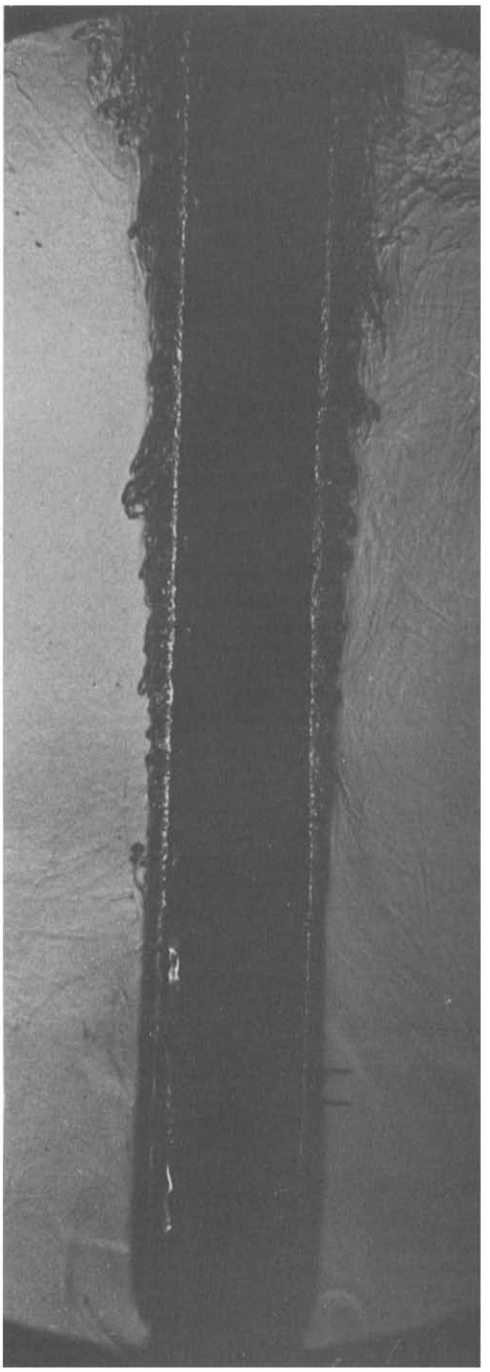

FIG. 1. Schlieren 'edge view' photograph of flow near vertical ice slab melting in saline water for $t_{\infty} = 1^{\circ}C$ using a vertical 'knife edge'. Instantaneous ice thickness projects approximately 3 mm beyond styrofoam frame.

Table 1. Downstream (upward) location, x, from lower 'leading edge' at which transition to turbulence was observed, along with three corresponding Grashof numbers for a range of ambient temperatures

t_∞ (°C)	x (cm)	$Gr_{x,\rho} \times 10^{-7}$	$Gr_{x,\beta} \times 10^{-7}$	$Gr_{x,\beta^*} \times 10^{-7}$
−0.07	16.5–22.2	5.9–14.5	0.039–0.094	6.0–14.0
1.0	12.8–14.9	7.5–11.8	0.063–0.098	7.6–11.7
2.8	9.2–11.3	4.3–8.0	0.053–0.099	4.3–8.0
5.3	8.5–9.3	4.5–5.9	0.096–0.126	3.7–4.9
9.4	5.5–6.4	1.5–2.4	0.066–0.111	1.5–2.6
13.4	4.6–5.5	1.0–1.7	0.070–0.130	1.0–1.8

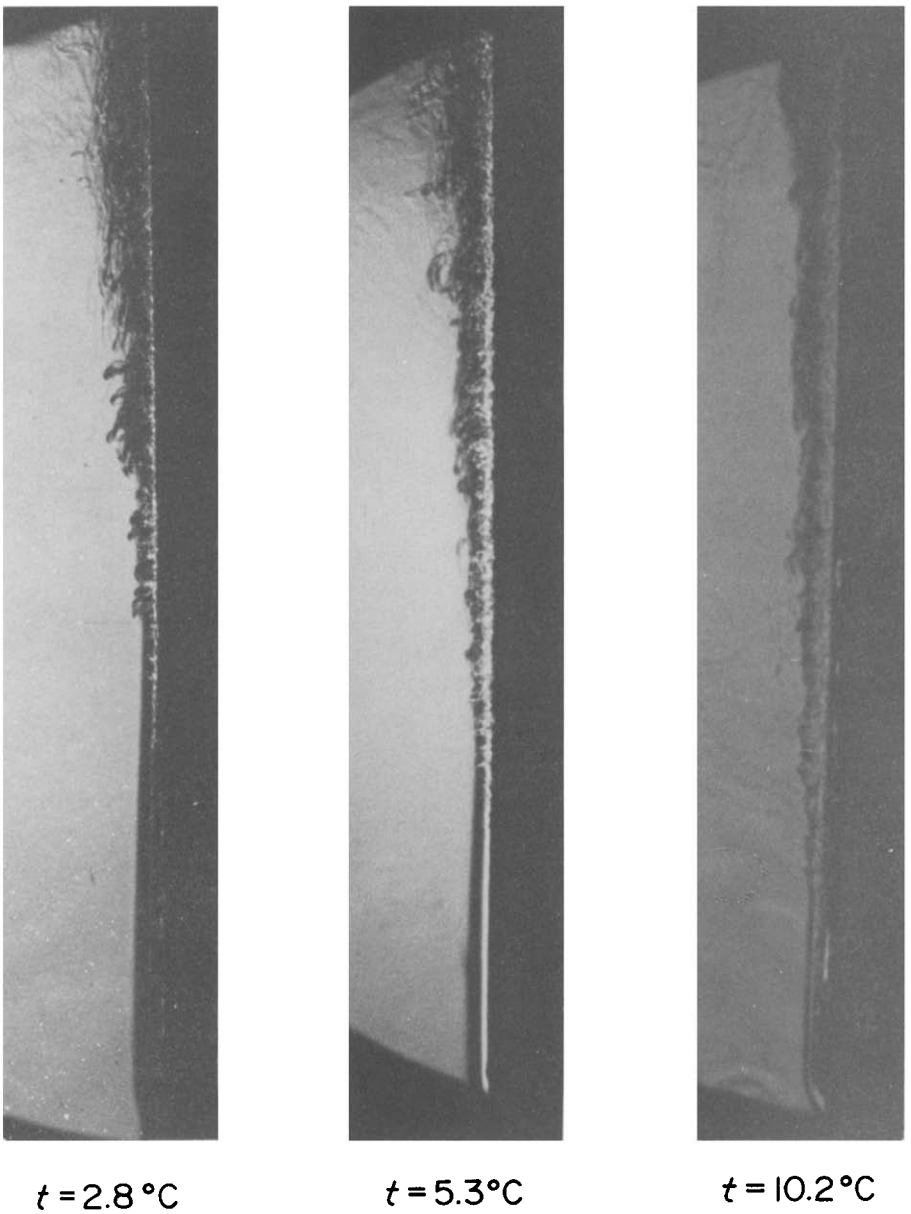

FIG. 2. Schlieren 'edge view' photographs showing flow near vertical ice slab melting in saline water for $t_\infty = 2.8$, 5.3, and 10.2°C using a circular diaphragm 'knife edge'.

$$Gr_{x,\rho} = \frac{gx^3}{\nu^2}\left(\frac{\rho_\infty - \rho_{il}}{\rho_r}\right) \quad (2a)$$

$$Gr_{x,\beta} = \frac{gx^3}{\nu^2}\beta(t_{il} - t_\infty)$$

where

$$\beta = -(1/\rho)(\partial\rho/\partial t)_{s,p} \quad (2b)$$

$$Gr_{x,\beta^*} = -\frac{gx^3}{\nu^2}\beta^*(s_0 - s_\infty)$$

where

$$\beta^* = (1/\rho)(\partial\rho/\partial s)_{t,p}. \quad (2c)$$

For comparison purposes, each of the Grashof numbers in equations (2a)–(2c) have been evaluated for the saline water experimental conditions here and are listed in Table 1. Values of β and β^* were calculated using the density relation of Gebhart and Mollendorf [17]. The saline Grashof number, equation (2c), most closely agrees with the density difference Grashof number, equation (2a). This implies that salinity effects on density dominate. It is also seen that $Gr_{x,\beta^*} - Gr_{x,\beta} = Gr_{x,\rho}$ to quite high accuracy.

A typical Schlieren photograph is shown as Fig. 1. The flow starts as laminar at the lower 'leading edge' and then develops quite rapidly into turbulence higher up the surface. From Fig. 2, the length of the laminar region can be seen to decrease with increasing t_∞. The x locations on the slab, from the lower 'leading edge', at which transition was observed are given in Table 1. Since transition is not distinct, a range of x is given for each ambient temperature along with corresponding values of three Grashof numbers.

In the present experiment, measured values of t_{il} were used to calculate the interface salinity from the equation of Fujino *et al.* [18]. It was found that for increasing t_∞ the interface salinity decreases toward zero [15], and is generally in agreement with calculations of Marschall [10] and the results of Josberger [7].

CONCLUSIONS

For the natural convection flow which arises during the melting of pure water ice in saline water, it was found that saline gradients dominate temperature gradients and determine ultimate flow direction. The net flow was found to be upward and turbulent for the experimental ambient temperature range -1.08 to 20.76°C. The flow began as laminar, then surprisingly rapidly developed into turbulence, with the length of the laminar region decreasing with increasing ambient temperature. The thickness of the laminar thermal boundary layer was seen to increase with downward distance from the laminar-to-turbulent transition location suggesting a bidirectional flow in the laminar region, as earlier reported by Josberger [7, 8] and Josberger and Martin [9]. It is suspected that the inherent contortion of such a bidirectional velocity profile is a highly destabilizing factor and results in the observed unusually early transition to turbulence. The melting rate was seen to decrease monotonically from 1.566 to 0.0035 g s^{-1} as t_∞ varied from 20.76 to -1.08°C. This represents a factor of 500 change in melt rate.

The interface salinity was found to increase and approach the ambient salinity for decreasing t_∞. The corresponding range of interface temperatures is from -0.10 to -1.76°C, with interface salinities ranging from 32.22 to 1.28‰. The experimental Nusselt number values, for the conditions studied here, were found to decrease monotonically with decreasing t_∞. No minimum was found as for ice melting into pure water. See Johnson [15] for details.

Using the frequency distribution of Antarctic icebergs observed by Gordienko [19] near Amery Ice Shelf and a six year lifetime as representative, Neshyba and Josberger [20] inferred an average sidewall melt of 45 cm day^{-1} and calculated 34 cm day^{-1} for $\Delta t = 2$°C. The present results suggest about 10 cm day^{-1} for $\Delta t = 2$°C. This is lower because of the absence of a much more extensive turbulent region which would be present in actual icebergs. These results are shown in Fig. 3. This puts the laboratory results in some perspective with actual iceberg melt rates.

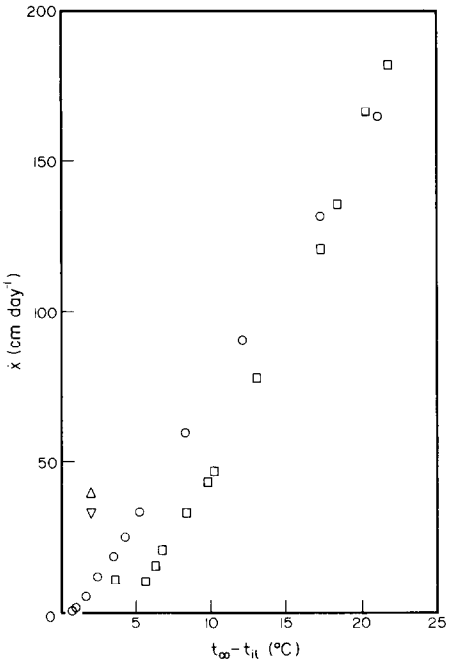

FIG. 3. Average sidewall melt. Present investigation plotted as: ○, $s = 35$‰; □, $s = 0$‰. Neshyba and Josberger [20]: △, inferred from Gordienko [19]; ▽, calculated.

Acknowledgements—The authors gratefully acknowledge grant support (ENG76-16936 and ENG77-27945) for this research from the National Science Foundation.

REFERENCES

1. J. S. Sandström. The hydrodynamics of the Canadian Atlantic waters, Canadian Fisheries Expedition (1919). Investigation in the Gulf of St. Lawrence and Atlantic waters of Canada (1914–1915).
2. S. Neshyba. Upwelling by icebergs, *Nature* **267**, 507–508 (1977).
3. V. P. Carey and B. Gebhart, Transport near a vertical ice surface melting in saline water: some numerical calculations. *J. Fluid Mech.* **117**, 379–402 (1982).
4. V. P. Carey and B. Gebhart, Transport near a vertical ice surface melting in saline water: experiments at low salinities, *J. Fluid Mech.* **117**, 403–423 (1982).
5. E. G. Josberger and S. Martin, Natural convective boundary layers adjacent to melting vertical ice walls in sea water. 56th Annual Meeting of the American Geophysical Union (1975).
6. E. G. Josberger, Laminar and turbulent boundary layers adjacent to melting vertical ice walls in sea water. 23rd Pacific Northwest Regional Meeting of the American Geophysical Union (1976).
7. E. G. Josberger, A laboratory and field study of iceberg deterioration, 1st Int. Iceberg Utilization Conf. (1977).

8. E. G. Josberger, Laminar and turbulent boundary layers adjacent to melting vertical ice walls, Ph.D. dissertation, Dept. of Oceanography, Univ. of Washington, Seattle, Washington (1978); see also ONR report 16, May (1979).
9. E. G. Josberger and S. Martin, A laboratory and theoretical study of the boundary layer adjacent to a vertical melting ice wall in salt water, *J. Fluid Mech.* **111**, 439–473 (1981).
10. E. Marschall, Free convection melting of glacial ice in saline water, *Lett. J. Heat Mass Transfer* **4**, 381–384 (1977).
11. J. Lyman and R. H. Fleming, Composition of seawater, *J. Mar. Res.* **3**, 134–146 (1940).
12. R. A. Cox, Chairman, Joint Panel on Oceanographic Tables and Standards, Unesco, Place de Fontenoy, Paris 7e, France (1966).
13. S. Neshyba, A comment on "On melting icebergs", by H. E. Huppert and J. S. Turner, *Nature* **275**, 567–568 (1978).
14. M. S. Bendell and B. Gebhart, Heat transfer and ice-melting in ambient water near its density extremum, *Int. J. Heat Mass Transfer* **19**, 1081–1087 (1976).
15. R. S. Johnson, Transport from a melting vertical ice slab in saline water, M.S. thesis, State University of New York at Buffalo, Amherst, New York (1978).
16. B. Gebhart and J. C. Mollendorf, Buoyancy-induced flows in water under conditions in which density extremum may arise, *J. Fluid Mech.* **89**, 673–707 (1978).
17. B. Gebhart and J. C. Mollendorf, A new density relation for pure and saline water, *Deep-Sea Res.* **24**, 831–848 (1977).
18. K. Fujino, E. L. Lewis and R. G. Perkin, The freezing point of sea water at pressures up to 100 bars, *J. Geophys. Res.* **79**, 1792–1797 (1974).
19. P. A. Gordienko, The role of icebergs in the ice and thermal balance of coastal Antarctic waters (transl.), *Problemy Arkt. Antark.* **2**, 17–22 (1960).
20. S. Neshyba and E. G. Josberger, Estimation of antarctic iceberg melt, *J. Phys. Oceanog.* **10**, 1681–1685 (1980).

Int. J. Heat Mass Transfer. Vol. 27, No. 10, pp. 1932–1935, 1984
Printed in Great Britain

0017 9310/84 $3.00 + 0.00

Burning of char/carbon particle in a periodic thermal environment

K. ANNAMALAI and S. STOCKBRIDGE

Department of Mechanical Engineering, Texas A and M University, College Station, TX 77843, U.S.A.

(*Received* 11 *July* 1983 *and in revised form* 17 *January* 1984)

NOMENCLATURE

A_H	heat transfer area
B	pre-exponential factor
C_p	specific heat of gas
D	diffusion coefficient
d_p	diameter of particle at any time
E	activation energy
h	heat transfer coefficient
h_m	mass transfer coefficient
M	mass
$\dot{M}$	mass rate
$\dot{M}_p$	mass rate of contact of solids with heat exchangers
n	see equation (5)
Nu	Nusselt number
Pr	Prandtl number
Re	Reynolds number
Sh	Sherwood number
T	temperature
ΔT_{BH}	temperature difference between bed and heat exchanger
ΔT_p	particle temperature drop near heat exchanger
t	time
t_p	period of time
t'_h	heating time available for each slug of mass in non-uniform temperature field in the free space
t_h	heating time available for char in uniform temperature field in the free space
W	weight
Y	mass fraction.

Greek symbols

δ	bubble void fraction
ν_s	stoichiometric coefficient for oxygen
ρ	density
σ	Stefan–Boltzmann constant.

Subscripts

b	burning
c	cooling or contact
ch	char
h	heating
nc	no contact
o	oxygen
p	particle
p,0	particle at time $t = 0$
R	radiation
s	solids (inert + char)
w	wall
∞	infinity.

1. INTRODUCTION

IN A FLUIDIZED bed combustor (FBC) fuel particles are introduced into a bed of sand (or dolomite and limestone) and burnt to release energy. A system of heat exchangers in the bed provides good control of the bed (or reaction zone) temperature within 1000–1200 K. As opposed to conventional combustion systems where heat exchangers are located away from the reaction zone and where the temperature of the reaction zone can be as high as 2000 K, the heat exchangers are